

Strain-controlled fatigue life and modeling of conduit polymers

Pei Chen · Shing-Chung Wong

Received: 24 May 2010 / Accepted: 21 October 2010 / Published online: 2 November 2010
© Springer Science+Business Media, LLC 2010

Abstract Strain-controlled fatigue lives of conduit polymers, viz., nylon 6, polypropylene (PP) and calcium carbonate filled black colored polypropylene (PP-blk) were studied. Thermal and mechanical analyses were conducted before fatigue tests. Thermal characteristics, such as the degree of molecular degradation, glass transition temperatures, and melting points were determined. Tensile strength, elastic modulus, and Poisson's ratio were obtained from tests under quasi-static loading. Fatigue lives were measured under different displacement ranges and temperature conditions. Four different temperatures were selected to represent low ($-40\text{ }^{\circ}\text{C}$), room ($25\text{ }^{\circ}\text{C}$), and high (65 and $125\text{ }^{\circ}\text{C}$) temperature conditions. Hysteretic heating was found to be significantly operative in PP specimens. By optimizing the previously developed unified strain model [1], strain fatigue lives were predicted based on the studied materials.

Introduction

Electrical conduits are used as carrier and protection for electrical and optical cables, and routing of electrical wiring. Engineering polymers [2] such as nylon and polypropylene (PP) exhibit considerable degradation life, high creep resistance, good durability, and insulator behavior. Of most critical interest is their cost-effectiveness, ease of fabrication and mass production, compared with metallic materials. PP, HDPE, PVC, and nylon serve as the materials of choice in conduit applications [3–5].

Strain fatigue failure is a predominant failure mode in wiring conduits, and a long fatigue life is preferred in engineering design. Applications of polymer conduits for this specific paper are subjected to straining instead of stress loading. The external mechanical loading causes large deformation of conduits, which includes both elastic and plastic deformations. Since stress controlled mode is not operative in the applications, strain-controlled mode is used to monitor the fatigue life. Results obtained from strain-controlled cycles cannot be directly extended to load-controlled fatigue. This is because the validity range for strain-controlled fatigue exceeds the range whereby linear elastic deformation is operative.

Polymer conduits experience cyclic strain for they are often designed for flexible and large deformation endurable purposes [6–8]. Most of the polymer fatigue tests were performed under stress or load-controlled mode in literatures [9–11]. Load-controlled fatigue tests are mostly used for materials with small deformation and for those that comply with linear elasticity. For materials with nonlinear deformation, strain-controlled fatigue tests are more applicable. Nevertheless, strain-controlled fatigue behavior of polymers is not well understood [12, 13] and the data available for strain fatigue deformation of polymers are sparse. This paper reports strain fatigue lives of conduit nylon 6 and PP. A model is proposed to address the experimental data. Previously, we reported the merits and applicability of a unified strain model in fatigues of PVC, PPE, and XLPE under controlled conditions [1, 14].

The Coffin–Manson model is the most widely cited model in predicting strain fatigue lives of metals [15, 16]. It has been used to predict composite fatigue lives [17, 18] and it can be shown in its simplified form as:

$$\Delta\varepsilon/2 = CN_f^{-m} \quad (1)$$

P. Chen · S.-C. Wong (✉)
Department of Mechanical Engineering,
The University of Akron, Akron, OH 44325-3903, USA
e-mail: swong@uakron.edu

where $\Delta\varepsilon$ is the total strain, N_f the number of cycles to failure, m and C are fatigue exponent and ductility coefficient, respectively. In order to incorporate mean stress/strain effects in fatigue damage, modified strain fatigue models were derived by investigators based on Coffin–Manson relationship, such as the Smith–Watson–Topper (SWT) parameter [19] and the Morrow mean stress model [20]. These models can make fatigue life prediction for metals taking into account of variable amplitude histories in a simple and practical way.

Recently, Wong and coworkers [1] derived a unified strain fatigue model, named Wei–Wong unified strain model, considering not only the mean strain effect, but also amplitude, maximum strain, and minimum strain effects, as shown below:

$$(\varepsilon_{\text{amp}} \times \varepsilon_m \times \varepsilon_{\text{max}} \times \varepsilon_{\text{min}})^{\frac{1}{4}} = CN_f^{-m} \tag{2}$$

where ε_{amp} , ε_m , ε_{max} , and ε_{min} are the absolute values of strain amplitude, mean strain, maximum, and minimum strains, respectively. This equation is broadly valid assuming tension–tension mode in fatigue cycles. The right hand side of Eq. 2 is the same as Coffin–Manson model. The Wei–Wong semi-empirical model combines the merits of single-parameter models, and minimizes the drawbacks of a single-parameter approach. The concept of a unified strain provides a new dimension in modeling fatigue life and presents opportunities for future work to validate such a model. In this paper, we will report an improved model based on the unified strain approach.

Experimental and modeling work

Materials and processing

The polymers used in this study are nylon 6, polypropylene (PP), and 20 wt% CaCO₃ modified polypropylene with black pigment (PP-blk). Nylon 6 was supplied by Delfingen US Inc. Both PP and PP-blk were supplied by Washington Penn Plastic Co. All of the three materials were obtained in the form of pellets. They were injection molded by Vandorn 55 injection molding machine into

ASTM 638D standard dog-bone specimens. PP and PP-blk do not need any drying process before injection molding. Nylon 6 is hygroscopic [21] and, therefore, dried at 100 °C for 24 h prior to injection molding. The injection molding parameters are shown in Table 1.

Thermal characterization

Thermogravimetric analysis (TGA) was used to determine the thermal degradations of molded specimens. The TGA 2050 from TA Instruments was utilized for measuring the weight loss as a function of temperature. Both the pellets and dog-bone specimens were tested separately to identify the effect of injection molding on the degradation behavior of polymers. Nitrogen is used to purge the TGA to prevent undesired reactions. The temperature increases from 25 to 600 °C (nylon 6) and 500 °C (PP and PP-blk) with a ramping rate of 30 °C/min.

Both the pellets and dog-bone specimens were studied using differential scanning calorimetry (DSC). The specimens were tested at temperatures ranging from 0 to 300 °C for nylon 6, and –50 to 300 °C for PP and PP-blk with a ramping rate of 10 °C/min.

A Perkin Elmer dynamic mechanical analyzer (DMA) was performed on molded specimens in tensile mode at a frequency of 10 Hz from –40 to 120 °C with a ramping rate of 4 °C/min. Liquid nitrogen was supplied for cooling.

Results from thermal analyses are summarized in Table 2.

Table 2 Physical properties: glass transition temperature, melting point, and degradation temperature for nylon 6, PP, PP (blk), respectively

	Glass transition temperature (°C)	Melting point (°C)	Degradation temperature (before/after molded) (°C)
Nylon 6	49	213	340/321
PP	3	158	370/365
PP-blk	–11	150	335/335

Table 1 Summary of parameters involved in the injection molding process

	Nylon 6	PP and PP-blk
Temperature at the front of the barrel	260 °C (500 F)	204 °C (400 F)
Max pressure	17 MPa (2500 psi)	17 MPa (2500 psi)
Holding pressure	2.8 MPa (400 psi)	2.8 MPa (400 psi)
Holding time	10 s	10 s
Temperature in the mold	27 °C (80 F)	77 °C (170 F)
Cooling time	35 s	35 s

Tensile tests

Uniaxial tensile tests are conducted using a quasi-static Instron 5582 machine at room temperature (25 °C). In order to determine the true stress–true strain relationships, two mechanical contact extensometers, viz., longitudinal and transverse extensometers, were used to measure the strains in longitudinal and transverse directions. A set of specimens were loaded at selected loading rates, 10, 20, 30, 40, 50, 60 mm/min for nylon 6; 20, 30, 40, 50, 75, 100 mm/min for PP and 40, 50, 75, 100, 150, 200 mm/min for PP-blk. The true stress (σ) of each sample can be obtained from [22]:

$$\sigma = \frac{P}{W_0 T_0 (1 - \varepsilon_z)^2} \quad (3)$$

where P is the applied load, W_0 and T_0 are the original width and thickness of the specimen, ε_z the transverse strain, which can be directly obtained from the transverse extensometer. With the high-precision extensometers employed, the elastic modulus and Poisson's ratio can be precisely determined from the true stress–true strain curves.

Strain-controlled fatigue tests

Specimens can be cyclically loaded under the endurance limit at small strains well beyond laboratory-observable conditions, that is, one test per week, for example. An initial pre-straining and mean strain are inadvertently used to shorten the testing time as machine hours permit. A cut-off point of 2 million cycles at room temperature is selected. Due to the limitation of liquid nitrogen, the low temperature test is restricted to less than 40,000 cycles. Fatigue tests are conducted under strain control in tensile mode. An Instron 8500 servo-hydraulic testing machine is employed at a frequency of 5 Hz.

In order to understand materials' mechanical response to cyclic loading, cyclic stress–strain curves are generated from initial cycles. Stress response is captured by computer from number 100–1000 loading cycles. Data from number 0–100 loading cycles is not used, because the machine has not reached the steady-state loading amplitude at the beginning cycles.

The fatigue failure tests are performed at four different temperature conditions, low temperature (−40 °C), room temperature (25 °C), high temperature (65 °C for PP and PP-blk, 125 °C for nylon 6). Nylon 6 has a high temperature resistance and the tests on nylon are performed at 125 °C. At each temperature, at least three data points are obtained in order to plot a strain-life cycle curve. All of the test data are displayed in Tables 3, 4, and 5 for nylon 6, PP, and PP-blk, respectively. During room temperature tests, a

Table 3 Summary of nylon 6 fatigue test data and materials constants

Temp (°C)	Amp (%)	Mean strain (%)	r	N_f	m	c
−40	3.12	3.13	1.00	18,200	0.68	136
	3.15	6.28	1.33	1,100		
	3.11	7.78	1.43	130		
25	2.72	4.66	1.26	552,200	0.13	9.9
	3.15	4.66	1.19	281,000		
	3.88	6.22	1.23	584,00		
125	7.1	139	1.90	453,000	0.34	11308
	7.36	241.21	1.94	72,400		
	6	359.3	1.97	30,300		

Table 4 Summary of PP fatigue test data and materials constants

Temp (°C)	Amp (%)	Mean strain (%)	r	N_f	m	c
−40	2.72	10.84	1.60	23,800	0.10	35.9
	2.36	14.15	1.71	21,400		
	2.34	23.39	1.82	50		
25	2.04	9.31	1.64	320,600	0.06	22.0
	2.91	9.31	1.52	132,900		
	4.07	9.31	1.39	88,100		
65	4.48	268.85	1.97	1,303,600	0.41	89269
	4.47	461.97	1.98	457,200		
	4.48	468.33	1.98	309,000		

thermal couple is attached to specimen's surface in order to monitor the temperature change.

Fatigue fractographic analyses

A Hitachi S-2150 scanning electron microscope (SEM) is employed to evaluate fractographic information of the specimens that fail by cyclical loading.

Modeling work

In the Wei–Wong unified model, a unified strain is a geometric mean value of four strain parameters: (1) mean strain, (2) maximum, (3) minimum strains, and (4) strain amplitude. The maximum and minimum strains are not independent variables and they depend on the chosen mean strain and thus the strain amplitude. Indeed, the mean strain and the strain amplitude are the only two independent parameters. Strain ratio is demonstrated to affect fatigue life [13, 23–25]. Larger strain ratio gives rise to shorter fatigue life. Here we propose a new modified strain fatigue life model, which is shown below:

Table 5 Summary of PP-blk fatigue test data and materials constants

Temp (°C)	Amp (%)	Mean strain (%)	<i>r</i>	<i>N_f</i>	<i>m</i>	<i>c</i>
-40	3.92	48.23	1.85	38,900	0.14	253.3
	3.98	63.78	1.88	31,600		
	3.96	137.49	1.94	65		
25	7	445.76	1.97	1,378,000	0.08	1428
	7.01	543.57	1.97	1,157,000		
	7.03	870.86	1.98	650		

$$\epsilon_u = \sqrt{r \times \epsilon_m \times \frac{\Delta\epsilon}{2}} = C \times N_f^{-m}, \tag{4}$$

where ϵ_u is the unified strain. $r = 1 + R$, where R is the absolute value of strain ratio. Equation 4 can be expressed in a log–log scale as follows:

$$\log(\epsilon_u) = -m \log(N_f) + \log(C) \tag{5}$$

In Eq. 5, $\log(\epsilon_u)$ has a liner relationship with $\log(N_f)$. All fatigue data can be analyzed linearly versus the unified strain.

Results and discussion

Molecular degradation

The relationship between mass loss of the sample and temperature increase is plotted for the studied specimens. Figure 1 shows the comparison of TGA results before and after processing for nylon 6, PP, and PP-blk, respectively. The degradation temperature is defined as the temperature at 5% weight loss. Nylon 6 has a degradation temperature of 340 °C before injection molding. Degradation temperature of nylon 6 decreases to 321 °C after injection molding. Similar phenomenon is observed on PP. Degradation temperature of PP decreases from 370 to 365 °C for the unmolded and molded samples. Degradation temperature of PP-blk has no change between the unmolded and molded samples, and it is consistently shown at 335 °C. Observation based on TGA from pellets with samples obtained through injection molding indicates that there is slight molecular degradation arising from the selected processing conditions.

Glass transition temperatures and melting points

Glass transition temperatures (T_g) of polymers are determined by DMA. Figures 2 and 3 show the variations of $\tan \delta$ and storage modulus as a function of temperature as determined by DMA. The T_g of nylon 6, PP, and PP-blk, are shown in Fig. 2, and they are 49, 3, and -11 °C, respectively. The

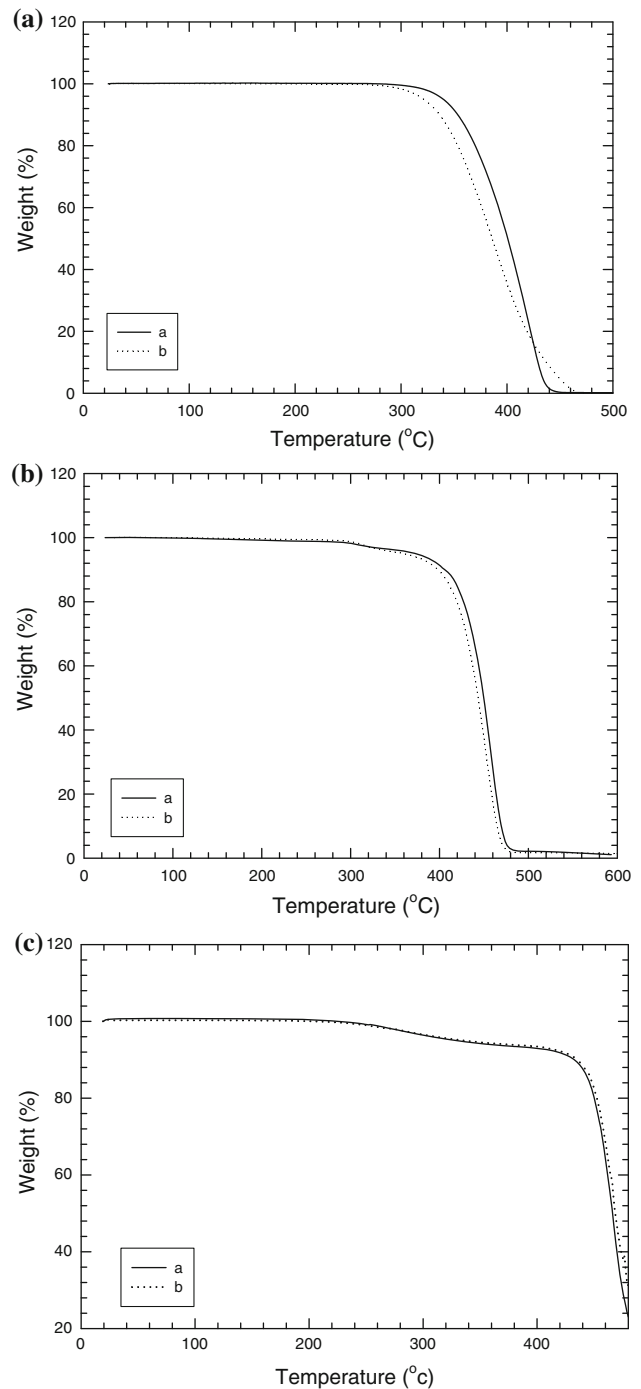


Fig. 1 Thermogravimetric analysis of nylon 6 (a), PP (b), and PP-blk (c). Change in weight (%) of sample with rise in temperature (°C) before injection molding (solid line a in each figure) and after injection molding (dotted line b in each figure). Minor molecular degradation is observed from the plots

literature values of T_g are 0 °C for PP and 47 °C for nylon 6. From Fig. 3, it is clear that PP and nylon 6 exhibit markedly higher storage moduli than PP-blk. Nylon 6 has a larger storage modulus above 0 °C than PP, but PP exhibits higher values than nylon 6 below 0 °C or above 47 °C.

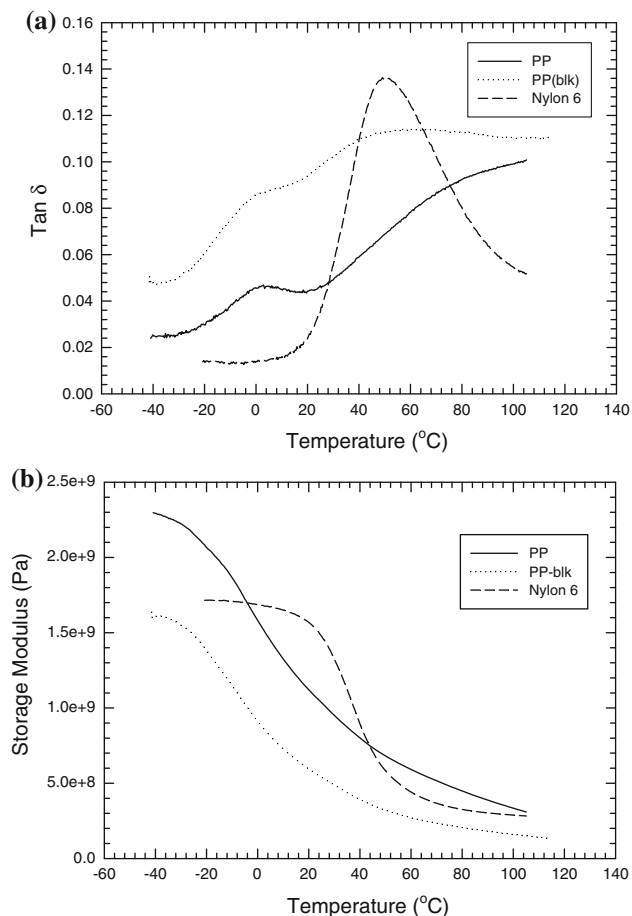


Fig. 2 Dynamic mechanical analysis of nylon 6, PP, and PP-blk. **a** Variation of $\tan \delta$ as a function of temperature. Glass transition temperature is obtained, at 49 $^{\circ}\text{C}$ (nylon 6), 3 $^{\circ}\text{C}$ (PP), and -11 $^{\circ}\text{C}$ (PP-blk). **b** Variation of storage modulus (E') as a function of temperature. E' decreases as temperature increases. PP has high E' than PP-blk in the whole temperature range

Melting temperature is the temperature range at which the state of polymer changes from solid to liquid states. Melting is an endothermic process, and that results in an endothermic peak in the DSC curve. From Fig. 3, melting points are found at 213, 158, and 158 $^{\circ}\text{C}$ for nylon 6, PP, and PP-blk, respectively. The integral of the peak is the heat of fusion. PP has the highest heat of fusion, followed by nylon 6. PP-blk has a similar melting point with PP, but the heat of fusion is drastically reduced due to substantially compromised crystalline phase and the inclusion of calcium carbonate.

True stress and true strain relationships

The true stress–true strain curves are obtained by using the longitudinal and transverse extensometers. Figure 4 shows the true stress–true strain relationships of nylon 6, PP, PP-blk at a loading rate of 50 mm/min. Clearly, nylon 6 is

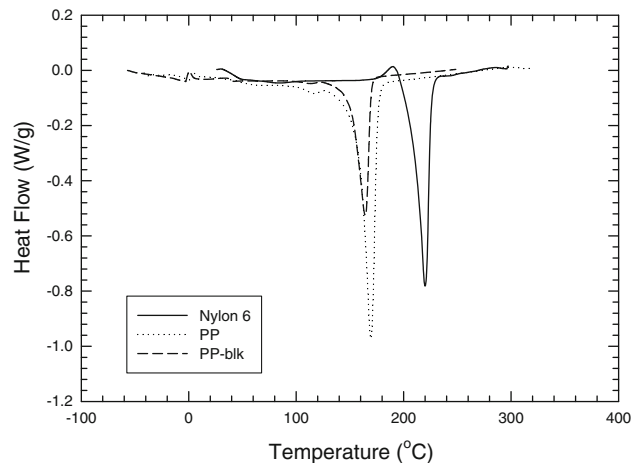


Fig. 3 Differential scanning calorimetry of nylon 6, PP, and PP-blk. Variation of heat flow as a function of temperature. Glass transition temperatures are obtained from the plots, at 35 $^{\circ}\text{C}$ (nylon 6), -2 $^{\circ}\text{C}$ (PP), and 5 $^{\circ}\text{C}$ (PP-blk) and melting point is 213 $^{\circ}\text{C}$ (nylon 6), 158 $^{\circ}\text{C}$ (PP), and 150 $^{\circ}\text{C}$ (PP-blk)

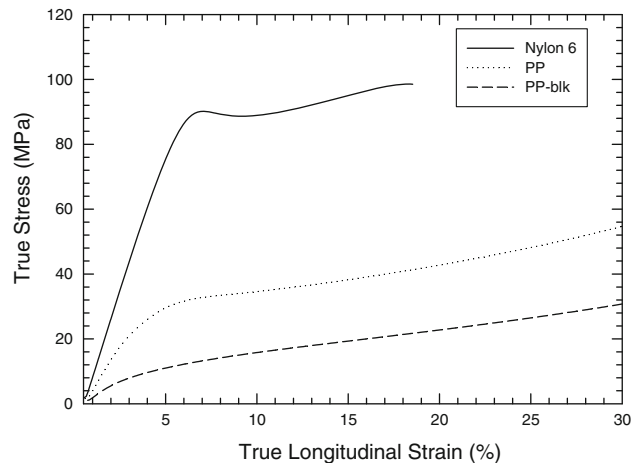


Fig. 4 True stress–true strain relationships at the loading rate of 50 mm/min for nylon 6, PP, and PP-blk. Nylon 6 is stiffer than PP, followed by PP-blk. The elastic moduli are 1.77, 0.98, and 0.33 GPa for nylon 6, PP, and PP-blk, respectively. The Poisson's ratios of nylon 6, PP, and PP-blk are 0.10, 0.18, and 0.19, respectively

significantly stiffer than PP, followed by PP-blk. Tests under different loading rates are performed, but the loading rate effect is insignificant. The elastic moduli are 1.77, 0.98, and 0.33 GPa for nylon 6, PP, and PP-blk, respectively. The Poisson's ratios of nylon 6, PP, and PP-blk are 0.10, 0.18, and 0.19, respectively. These values are highly reproducible and they are independent of the applied loading rates.

Elastic moduli from literatures are 2.6–3.0 GPa for nylon 6 and 1.5–2 GPa for PP, which are higher than values obtained from our laboratory. Poisson's ratios from literatures are 0.39 for nylon 6 and 0.36 for PP. One

possible explanation for the difference between our experimental and reported values in literatures is the materials we used are processed and optimized for conduit applications. Low elastic moduli indicate our conduit materials are softer, and conducive to straining. By minimizing Poisson's effect, conduits can retain their cyclical shape constantly.

Strain-controlled fatigue tests

Cyclic stress–strain behavior at ambient temperature

Typical cyclic stress–strain response of nylon 6, PP, and PP-blk under room temperature was shown in Fig. 5a–c. All of these tests are under constant strain amplitude with tension mean strain level. Most area of the hysteresis loop is under tension range; therefore, most of the hysteresis energy is generated by tension. Surface temperature is monitored and recorded in Fig. 6.

The shape of the hysteresis loop is varying cycle by cycle which evidences an increase in thermodynamically irreversible damage in the specimen [26]. Thermal damage can accelerate materials fatigue failure accompanied with mechanical damage [27, 28]. Nylon 6, as shown in Fig. 5a, has stable hysteresis loops, and so does PP-blk, as shown in Fig. 5c. Stable hysteresis loops mean energy dissipation and generation reach a dynamic equilibrium and therein specimens will not be significantly heated by hysteresis energy. In Fig. 6, after 1200 cycles, the temperatures of nylon 6 and PP-blk are in dynamic equilibrium at 46 and 35 °C, respectively. Therefore, thermal damage in nylon 6 and PP-blk is not clearly evident, and mechanical damage is the main mechanism for fatigue failures.

Figure 5b shows the hysteresis loops of PP which vary cycle to cycle. And stress decreases significantly as cycles advance. The area of hysteresis loop is also reduced obviously. In Fig. 6, PP is heating rapidly from 25 to 67 °C in the initial 1200 cycles, and after 2000 cycles temperature reaches a plateau at 50 °C. Temperature increases with PP producing softening effect. Therefore, thermal heating or melting plays an important role in the fatigue process.

Fatigue tests under different temperatures

Three different temperatures for nylon 6 specimens are –40, 25, and 125 °C and those for PP and PP-blk are –40, 25, and 65 °C. Since 65 °C is close to nylon 6's T_g (49 °C), in order to obtain high temperature fatigue behaviors which differ from brittle phase, nylon 6 was tested at 125 °C instead of 65 °C. Plots of the unified strains versus fatigue lives in log–log scale are shown in Fig. 7a–c based on the new empirical model we propose for these conduit polymers. Table 3 shows fatigue test conditions and results of nylon 6. The

fatigue exponents and ductility coefficients fitting new empirical model are also summarized. Table 4 shows fatigue test results of PP. Table 5 shows fatigue tests of PP-blk under two temperature conditions, since no PP-blk fracture is observed at 65 °C. It is clear that the new unified strain model can fit all data well with high precision. Note that the data shown on Fig. 7 cannot be directly applied or extended to stress- or load-controlled fatigue cycles. This is because the range of deformation as shown in Fig. 7 exceeds the validity range of linear elastic deformation. The relationship between stress and strain becomes a variable as fatigue cycle increases. The comparison between this new and Wei–Wong models will be discussed in the following section.

Temperature effects are observed among low, room, and high temperature tests. The common trend is unified strain and fatigue life increase with temperature. All of the low temperature tests are conducted under materials' glass transition temperatures, therefore, molecular mobility is restricted and the polymers become brittle. Specimens under glass transition endure lower strains and shorter fatigue lives than specimens under room temperature, as observed from Fig. 7a–c. Tested specimens accommodate significantly higher unified strain and longer fatigue life at high temperatures except nylon 6. Nylon 6 possesses a high unified strain, which implies a transition from brittle to ductile behaviors. But ductile nylon 6 does not exhibit better fatigue life under high temperature conditions. It was reported that nylon 6 exhibits lower heat diffusivity ($\sim 0.09 \text{ mm}^2/\text{s}$) than PP ($\sim 0.28 \text{ mm}^2/\text{s}$) [29, 30]. As a result, the high temperature fatigue performance of nylon 6 can be attributed to hysteretic heat accumulation during testing. Ambient temperature can possibly attenuate heat dissipation rate, and temperature increases rapidly locally. Therefore, fatigue fracture is induced by over-heated zone.

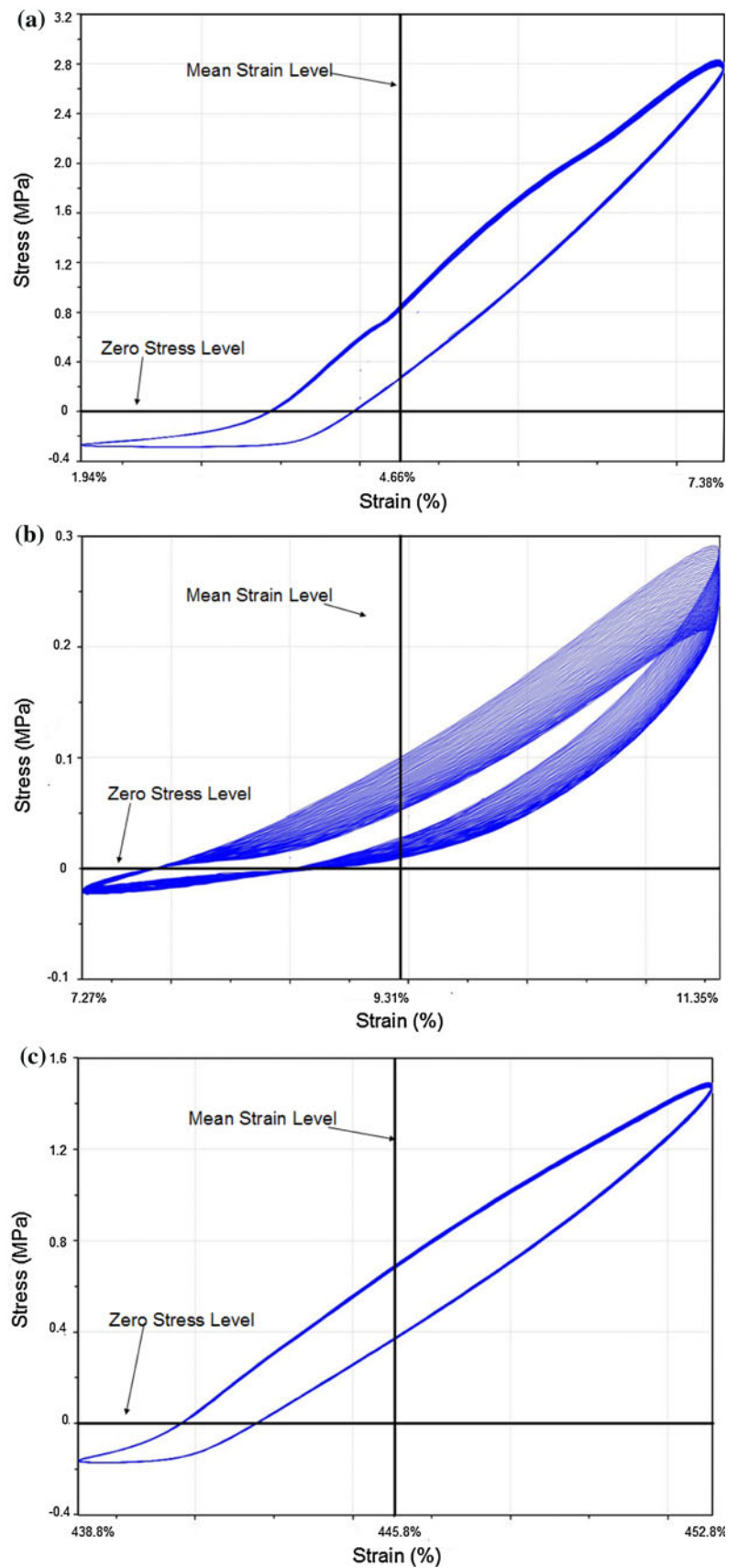
PP under low and room temperatures exhibit similar fatigue lives, and better fatigue behavior is observed under high temperature. Two predictive equations derived from low and room temperature tests have the similar fatigue exponents (m) and fatigue ductility coefficients (C), which indicate no significant change in fatigue life exists between specimens tested under low and room temperatures.

PP-blk possesses best fatigue behavior compared with nylon 6 and PP. Fatigue life of PP-blk at room temperature is comparable with those of nylon 6 and PP under high temperatures, in terms of unified strain or cycles to failure. PP-blk exhibits infinite fatigue life under high temperature. In high temperature tests, no fracture is observed under testing machine's capacity and within our cut-off time.

Post-failure fractographic analyses

Dissimilar to metal fatigue mechanisms of crack initiation and propagation or stress concentration, polymer fatigue

Fig. 5 Cyclic stress–strain relationships of **a** nylon 6, **b** PP, and **c** PP-blk under room temperatures in strain-controlled mode. The *horizontal solid dark line* in each figure is the zero stress level, the *vertical solid dark line* in each figure the mean strain level, and all of the mean strains in **a**, **b**, and **c** are tensile strains



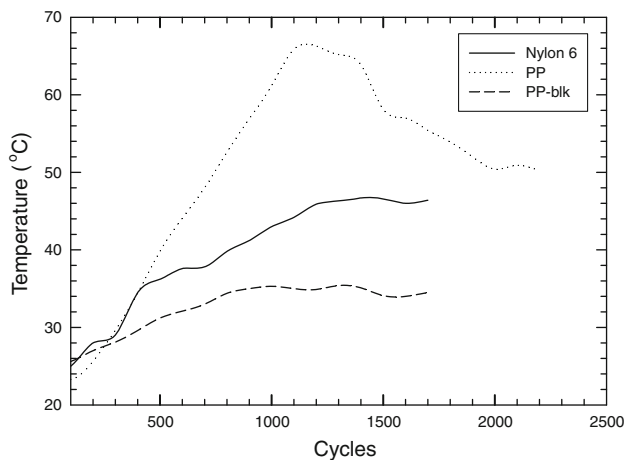


Fig. 6 Effect of specimen surface temperature on the initial loading cycles under room temperatures. The surface temperature of nylon 6 increases from 25 to 46 °C in 0–1200 cycle, and then keeps at 46 °C constantly after that. The surface temperature of PP increases from 25 to 67 °C in 0–1000 cycle, then decreases from 67 to 50 °C from 1000 to 2000 cycle. After that, the temperature remains constant at 50 °C

operates partially by hysteretic heat [31, 32]. Viscous damping or hysteresis generates heat, which softens or melts materials locally, and causes fracture directly or indirectly by accelerating crack initiation and propagation. Using post-mortem fractographic examinations, different fracture patterns, and hysteretic heating characteristics can be identified.

Figure 8a shows a digital image of nylon 6. The upper and lower sections of the surface display different patterns, as divided by a white dashed line, as shown in Fig. 8a. Section A shows fine striations which are formed by cyclical loading, and section B shows tearing and debonding. Cyclical loading, which produces the striations, affects section A first. Following the failure of section A, stress is concentrated on the ligament, section B. With plausible non-uniform melt flow in the central region of cavity during injection molding, stress concentration is exacerbated by non-uniform dispersions and thus tearing of the remaining ligament rapidly.

Brittle metals often exhibit striation markings at 500 to 2,500× [33]. One striation is formed during one successful loading cycle; therefore, the number of striations indicates the number of fatigue cycles. Figure 8b is taken at 150× magnification in section A, which is lower than the magnification required for observing striations in metals. But the striation marking is clearly observed at this magnification. Striations in nylon 6 are obscured by local softening and melting due to hysteretic heating, and thus the number of striations cannot reflect the number of fatigue cycles. In Fig. 8c, sub-critical markings are found on each striation. This is evidence for striation relaxation by heat.

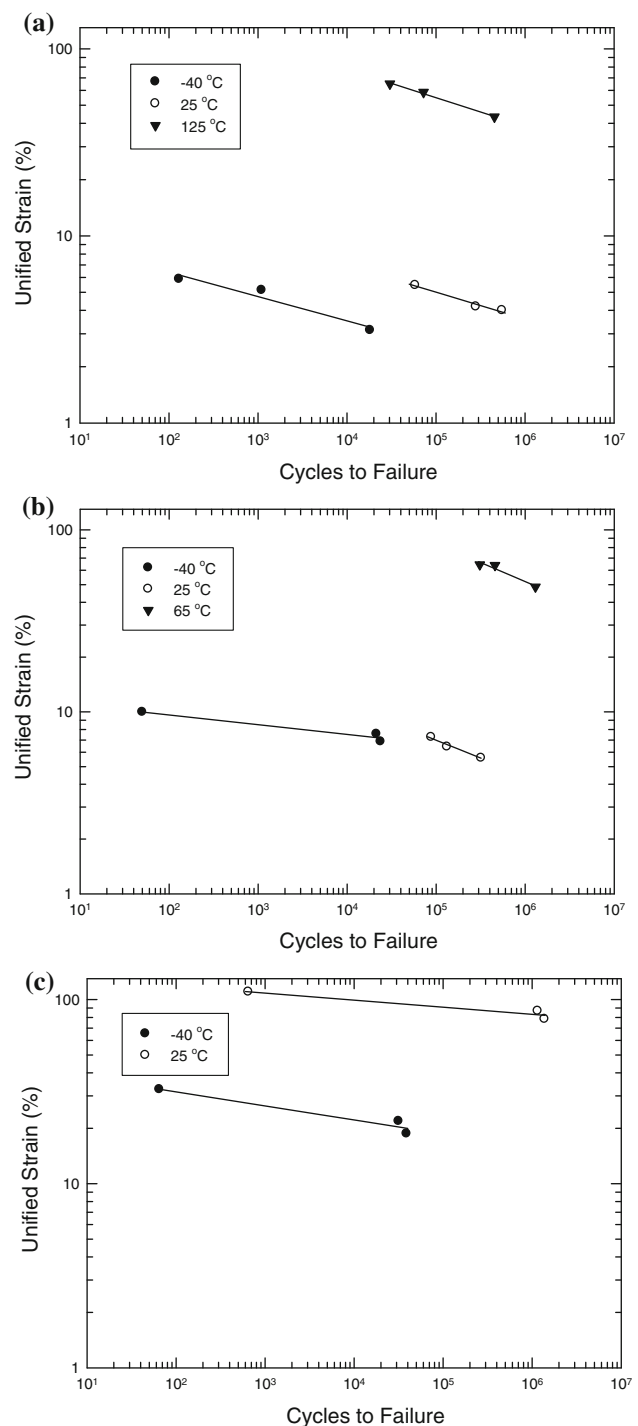


Fig. 7 Fatigue life prediction based on Wei–Wong–Chen unified strain model. **a** Nylon 6 fatigue life under –40, 25, and 125 °C; **b** PP fatigue life under –40, 25, and 65 °C; **c** PP-blk fatigue life under –40 and 25 °C

PP has a coarse fracture surface which is shown in Fig. 9a. Zok and Shonozaki [34] demonstrated segmented crazes form during the initial cycles of fatigue tests in polymers, and the crazes are parallel to the loading direction. As the number of cycles increases, the size of crazes

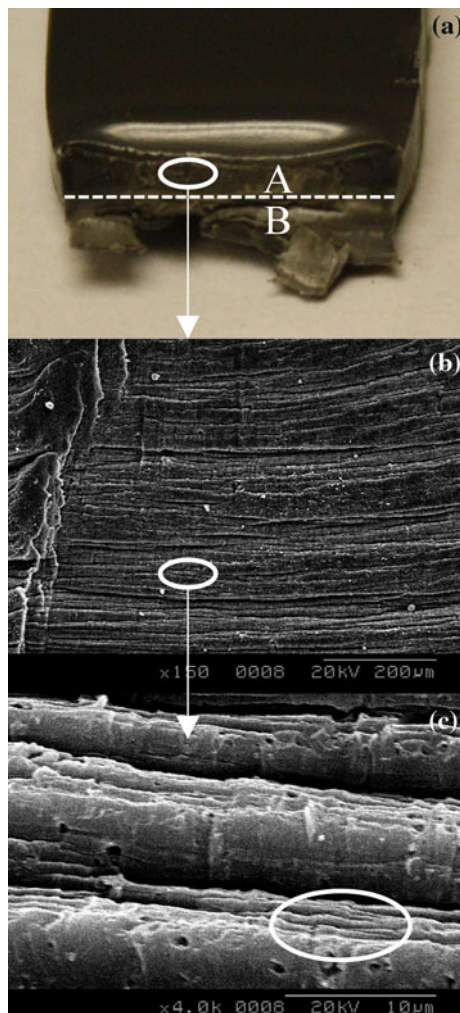


Fig. 8 Fatigue fracture surface of nylon 6 under different magnifications. **a** Digital image of fracture surface. Sections *A* and *B* are divided by a *white dashed line*. Section *A* shows striation markings. Section *B* shows debonding and pulled-out flakes. **b** Enlarged micrograph of section *A*. Striation markings display uniform spacing. **c** Enlargement of striation markings. Several markings are found in each striation. This indicates that some striations in nylon 6 are obliterated by melting due to hysteretic heat

increases; therefore, the crazed segment remains as the load-bearing ligament. With an elevated stress concentration, the craze segments fracture, and eventually lead to massive debondings and thus flake-like (a debonded structure) features on micrographs. If we carefully examine the fracture surface as shown in Fig. 7b at high magnification, some slight fatigue striations can still be observed, but they are not as distinct as the ones appearing in nylon 6.

PP-blk shows a more featureless fracture surface with some striation markings, as shown in Fig. 10. No debonded flake is seen like PP's. The loaded region in Fig. 10 is immediately prior to complete failure of a specimen. The featureless fracture surface indicates no significant crazed or debonding zone. In comparison to nylon 6 in Fig. 8, the

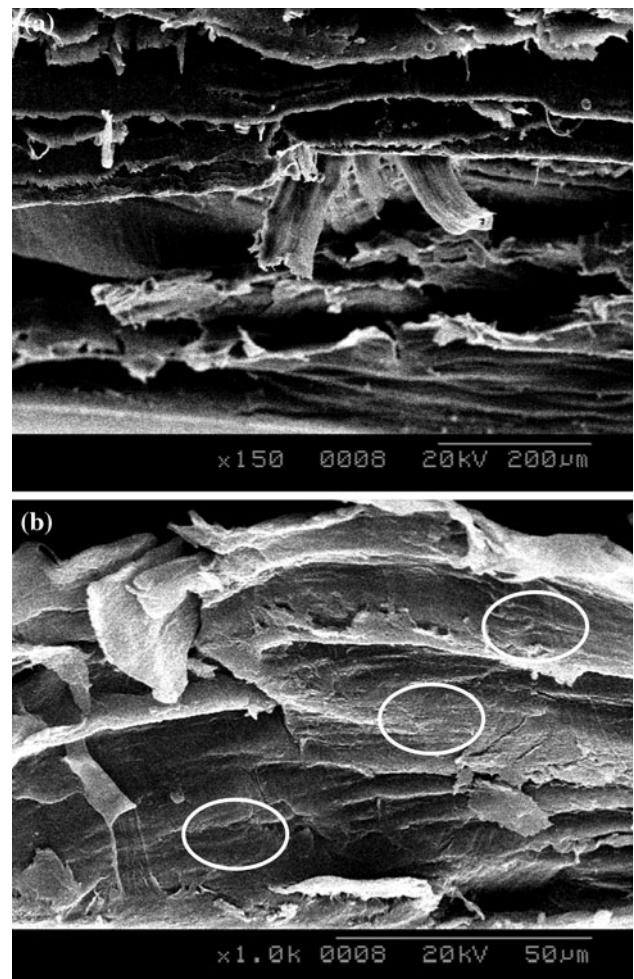


Fig. 9 Fatigue fractograph of PP. **a** Cross-sectional view of fracture surface. Fractograph shows massive debonding with pull-out flakes. **b** Some slight striations are observed at higher magnification, as indicated by *circles* in the figure

width of striation in PP-blk is roughly 5–10 times larger than the striation width of nylon 6; and nylon 6 striations are more legible than PP-blk striations. Accumulated hysteretic heat primarily obliterates the striations in PP-blk.

The conclusions from post-failure fractographs are consistent with our hysteresis loop discussions from “[Cyclic stress–strain behavior at ambient temperature](#)” section. PP exhibits the most severe self-heating problem. Nylon 6 and PP-blk have stable hysteresis loops and therefore thermal damage is considered less significant. Additionally the striations in their surface show a trace of mechanical damage.

New empirical unified strain model

Coffin–Manson model is often cited for metals. The Coffin–Manson depends on the statistical nature of crack nucleation within grains at the surface of polycrystalline

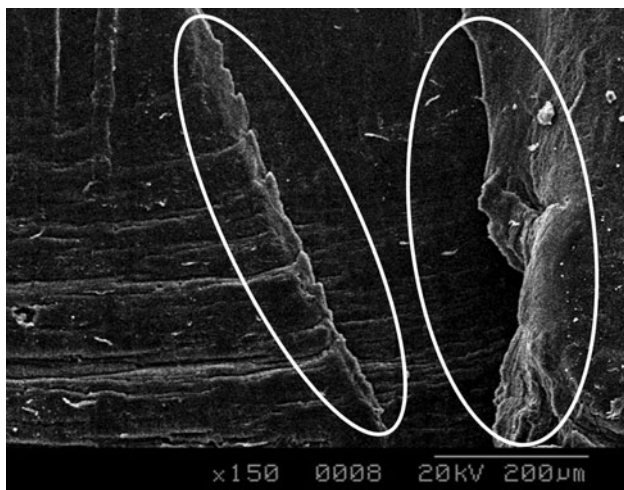


Fig. 10 Fatigue fractograph of PP-blk. Fracture surface is more featureless with several wide and finer striations. Stress concentration region is found on the surface, as indicated by white circles

materials [35]. However, no physical basis is provided to support the view of this model is applicable to polymers.

The two widely recognized mean stress/strain models on metallic materials are Smith–Watson–Topper (SWT) mean stress model [19] and Morrow mean stress model [20]. Both of these two models are based on the mechanism of Coffin–Manson relationship. The SWT model is shown in Eq. 6, and Morrow model in Eq. 7, as follows:

$$\sigma_{\max} \frac{\Delta \epsilon}{2} = \frac{\sigma_f'^2}{E} (2N_f)^{2b} + \sigma_f' \epsilon_f' (2N_f)^{b+c} \quad (6)$$

$$\frac{\Delta \epsilon}{2} = \frac{\sigma_f' - \sigma_0}{E} (2N_f)^b + \epsilon_f' (2N_f)^c \quad (7)$$

where σ_f' and ϵ_f' are the fatigue coefficients, respectively, b and c the fatigue exponents, and σ_0 the mean stress. Morrow proposed that the mean stress only affects the elastic portion of the strain-life curve. But during fatigue tests under large deformation, plastic strain exists and cannot be ignored. In these two models, mean stress, maximum stress, and elastic modulus are required as constant values, but they are varying cycle by cycle when testing polymers with large deformation, which are known as cyclic softening and hysteretic heating. Significant errors can exist if values of mean stress, maximum stress and elastic modulus are considered as constant [18].

Based on our previous Wei–Wong unified strain model, the improved empirical strain model, as shown in Eq. 4, is used to predict fatigue life. From Fig. 7a–c, all of the data are fitted well by the improved empirical model. The errors are calculated and shown in Fig. 11. In the figure, a solid diagonal line presents perfect prediction and the dash lines on either side represent the error bands of one order of magnitude. Most of the data points lay on the diagonal solid line. Fatigue lives of PP (–40 °C), PP-blk (–40 °C),

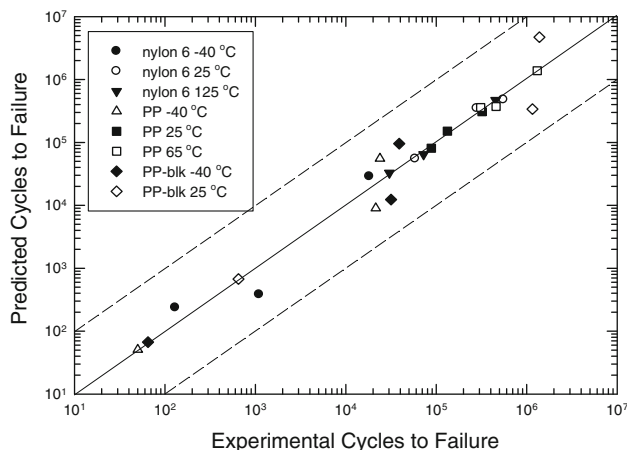


Fig. 11 Error analysis of fatigue life predicted by an improved unified strain model. Solid diagonal line represents perfect prediction, and the dashed lines on either side represent the error bands of a factor of 10. Most of the data points lay on the solid diagonal line; no data represent any error beyond the error bands of one order-of-magnitude

and PP-blk (25 °C) are not well predicted. Although these three tests are not perfectly consistent, the errors of them still fall within the error bands of one order of magnitude.

Since Coffin–Manson model is highly cited in the fatigue studies for metals, it is used to fit our data. The accuracy of Coffin–Manson model, Wei–Wong model and the improved unified strain model, hereby named Wei–Wong–Chen model, is evaluated by the coefficient of determination (R^2) based on our experimental data, as shown in Fig. 12. R^2 gives the proportion of the variance of

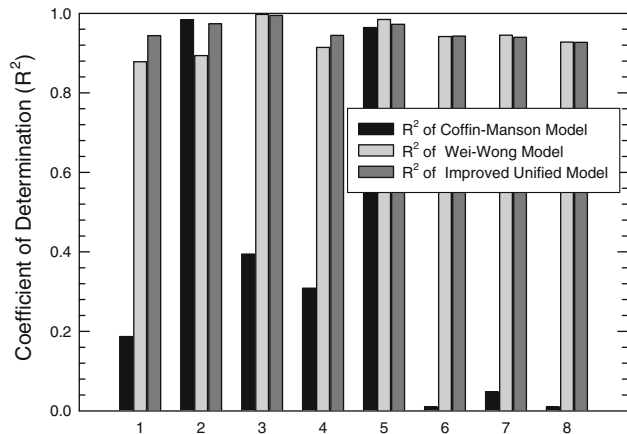


Fig. 12 Comparison of Wei–Wong model and the new improved model. X axis represents the catalog of eight fatigue life predictions, nylon 6 (–40 °C), nylon 6 (25 °C), nylon 6 (125 °C), PP (–40 °C), PP (25 °C), PP (65 °C), PP-blk (–40 °C), and PP-blk (25 °C) in a consequence of number 1–8. Y axis represents the coefficient of determination (R^2) of the linear regression of the data. Both Wei–Wong model and improved unified model have good prediction accuracy. The improved model exhibits better prediction than Wei–Wong model in the tests of (i) nylon 6 (–40 °C), (ii) nylon 6 (25 °C), and (iii) PP (–40 °C)

fatigue life that is predictable from unified strain, such that $0 \leq R^2 \leq 1$. R^2 represents the goodness fit of the fatigue data. Figure 12 shows the comparison of R^2 based on the Coffin–Manson model [15, 16], Wei–Wong model [1] and the new improved empirical, Wei–Wong–Chen model. The Coffin–Manson model is a single-parameter model. Only the strain amplitude is considered in this model, and the mean strain effect cannot be represented. If the mean strain is constant and the amplitude is a variable parameter, the Coffin–Manson model will give a good fit, such as in PP (25 °C) tests. The Wei–Wong model and the new improved model are multiple-parameter models. None of R^2 from Wei–Wong model and the improved model is below 0.8. The new model shows a better fit than Wei–Wong model on nylon 6 (–40 °C), nylon 6 (25 °C), and PP (–40 °C). Their correlations are consistent with the Wei–Wong model on nylon 6 (125 °C), PP (25 °C), PP (65 °C), PP-blk (–40 °C), and PP-blk (25 °C). As a result, the new improved Wei–Wong–Chen model possesses a greater applicability to the reported data, even though it is a three-parameter concept whereas the Wei–Wong model requires four parameters.

Conclusions

The following conclusions can be drawn from our studies:

- (1) Generally polymers show higher fatigue lives and higher strain endurance at higher temperatures during displacement-controlled fatigue tests.
- (2) Nylon 6 is much stiffer and stronger than PP and PP-blk. Nylon 6 possesses the worst fatigue properties among the three studied materials.
- (3) Fatigue property of PP under room temperature is similar under low temperature.
- (4) PP-blk provides the best fatigue life. No failure is observable under high temperatures and laboratory conditions.
- (5) Fatigue failure of Nylon 6 and PP-blk is mainly caused by mechanical damage. Thermal damage on PP by hysteretic heating is the primary mechanism for fatigue failure.
- (6) An improved unified strain model, named Wei–Wong–Chen model, derived from the previous Wei–Wong unified strain model shows greater correlation with the experimental data and merits for fatigue life prediction for conduit polymers.

References

1. Wei X, Wong SC, Bandaru S (2009) *J Mater Sci* 45:326. doi: [10.1007/s10853-009-3938-1](https://doi.org/10.1007/s10853-009-3938-1)
2. Chester G (1956) *Plast Technol* 2:594
3. Sillars RW (1973) Electrical insulating materials and their application. Peter Peregrinus Ltd, Stevenage, England
4. Gaube F, Muller W, Diedrich G (1971) *Chem Eng World* 10:39
5. Germain Y (1998) *Polym Eng Sci* 38:657
6. Branco CM, Rosa LG (1989) *Advances in fatigue science and technology*. Springer, Dordrecht
7. Regel VR, Leksovsky AM (1967) *Int J Fatigue* 3:99
8. Sauer JA, Richardson GC (1980) *Int J Fract* 16:499
9. Beardmore P, Rabinowitz S (1974) *Appl Polym Symp* 24:25
10. Sauer JA, Foden E, Morrow DR (1977) *Polym Eng Sci* 17:246
11. Helmi K, Fam A, Mufti A (2008) *J Compos Constr* 12:212
12. Tao G, Xia Z (2007) *Int J Fatigue* 29:2180
13. Meziere Y, Bunsell AR, Favry Y, Teissedre JC, Do AT (2005) *Compos Part A* 36:1627
14. Wong SC, Bandaru S (2009) *J Mater Sci* 44:356. doi: [10.1007/s10853-008-3152-6](https://doi.org/10.1007/s10853-008-3152-6)
15. Coffin LF (1954) *Trans ASME* 76:931
16. Manson SS (1965) *Exp Mech* 5:193
17. Opp DA, Skinner DW, Wiktorek RJ (1969) *Polym Eng Sci* 9:121
18. Kallmeyer AR, Stephens RI (1995) *J Compos Mater* 29:1621
19. Smith KN, Watson P, Topper TH (1970) *J Mater* 5:767
20. Morrow JD (1968) *Fatigue design handbook—advances in engineering*, vol 4. Society of Automotive Engineers, Warrendale, p 21
21. Monson L, Braunwarth M, Extrand CW (2007) *J Appl Polym Sci* 107:355
22. Nair SV, Wong SC, Goettler LA (1997) *J Mater Sci* 32:5335. doi: [10.1023/A:1018618912039](https://doi.org/10.1023/A:1018618912039)
23. Xiao X (2008) *Polym Test* 27:284
24. Huang CS, Wanga SH, Wua CC, Huang YS, Fang J (2006) *Scr Mater* 54:1181
25. Lin CK, Huang CM (2006) *J Electron Mater* 35:292
26. Wang SS, Chim ES-M (1983) *J Compos Mater* 17:114
27. Shen X, Xia Z, Ellyin F (2004) *Polym Eng Sci* 44:2240
28. Lesser AJ (1995) *J Appl Polym Sci* 58:869
29. Weidenfeller B, Hofer M, Schilling FR (2004) *Compos Part A* 35:423
30. Holman JP (2002) *Heat transfer*, 9th edn. McGraw-Hill, New York
31. Riddell MN, Koo GP, O'Toole JL (1966) *Polym Eng Sci* 6:363
32. White JR, Teht JW (1979) *Polymer* 20:764
33. Parrington RJ (2002) *Pract Fail Anal* 2:16
34. Zok F, Shonozaki DM (1987) *J Mater Sci* 22:3995. doi: [10.1007/BF01133350](https://doi.org/10.1007/BF01133350)
35. Sornett D, Magnin T, Breche Y (1992) *Europhys Lett* 20:433